View metadata, citation and similar papers at core.ac.uk

brought to you by CORE

provided by Elsevier - Publisher Connector

Available online at www.sciencedirect.com

SCIENCE DIRECT®

Virology 320 (2004) 276–290

VIROLOGY

www.elsevier.com/locate/yviro

Red clover necrotic mosaic virus replication proteins accumulate at the endoplasmic reticulum

Katherine A. Turner,[a,1] Tim L. Sit,[b] Anton S. Callaway,[c] Nina S. Allen,[c] and Steven A. Lommel[a,b,*]

[a] *Department of Genetics, North Carolina State University, Raleigh, NC 27695-7614, USA*
[b] *Department of Plant Pathology, NC State University, Raleigh, NC 27695-7616, USA*
[c] *Department of Botany, NC State University, Raleigh, NC 27695-7613, USA*

Received 5 November 2003; returned to author for revision 9 December 2003; accepted 11 December 2003

Abstract

Red clover necrotic mosaic virus (RCNMV) encodes N-terminally overlapping proteins of 27 and 88 kDa (p27 and p88) known to be required for replication. Green fluorescent protein (GFP) fusions were used to visualize the location of p27 and p88 within *Nicotiana benthamiana* cells. GFP:p27 fusions localized to the endoplasmic reticulum (ER), co-localized with ER-targeted yellow fluorescent protein and caused membrane restructuring and proliferation. Cellular fractionation of virus-inoculated *N. benthamiana* leaves confirmed the association of p27 with ER membranes. GFP:p88 fusions also localized to the ER and co-localized with GFP:p27. Both fusion proteins co-localize to the cortical and cytoplasmic ER and were associated with invaginations of the nuclear envelope. Independent accumulation in, and perturbation of, the ER suggests that p27 and p88 function together in the replication complex. This is the first report of a member of the *Tombusviridae* replicating in association with the ER.
© 2004 Elsevier Inc. All rights reserved.

Keywords: RCNMV; Polymerase; Green fluorescent protein; Endoplasmic reticulum; Co-localization; *Tombusviridae*; Confocal microscopy

Introduction

Replication is the critical step in the viral infection cycle, and as such, is often the target of anti-viral strategies. Much research focuses on the conserved aspects of replication, including viral and host factors, and cellular localization. Some virus genera replicate in hosts from multiple kingdoms (Janda and Ahlquist, 1993; Selling et al., 1990; Wijkamp et al., 1993), suggesting that host components that contribute to the replication complex are conserved across kingdoms. The fact that widely divergent virus families share form and function of replication strategies suggests that elucidating these processes for one virus will provide insight to virus life cycles in general.

A feature common among positive-strand RNA viruses is a requirement for replication in association with host membranes (Carette et al., 2000; Lee et al., 2001; Miller et al., 2001; Restrepo-Hartwig and Ahlquist, 1999; Rohozinski and Hancock, 1996). The presence of a replicating virus frequently induces proliferation and rearrangement of the host membranes (Bong et al., 1999; Reichel and Beachy, 1998; Rohozinski and Hancock, 1996; Rubino et al., 2000). The specific type of membrane system utilized in assembling the viral replication complex depends on the individual virus and is likely to be genetically determined (Burgyan et al., 1996; Hagiwara et al., 2003; Rubino and Russo, 1998). However, the specific membrane targeted by the polymerase may not be critical for replication as several RNA virus replication complexes have been retargeted to other membranes without loss of function (Burgyan et al., 1996; Miller et al., 2003). Picorna-like plant virus polymerase proteins (Carette et al., 2000; Schaad et al., 1997) as well as α-like plant virus polymerases (dos Reis Figueira et al., 2002; Dunoyer et al.,

* Corresponding author. Department of Plant Pathology, North Carolina State University, Box 7616, Raleigh, NC 27695-7616. Fax: +1-919-515-7716.

E-mail address: steve_lommel@ncsu.edu (S.A. Lommel).

[1] Present address: Gene Regulation and Chromosome Biology Laboratory, National Institutes of Health, NCI-Frederick, PO Box B, Frederick, MD 21702.

0042-6822/$ - see front matter © 2004 Elsevier Inc. All rights reserved.
doi:10.1016/j.virol.2003.12.006

2002; Mas and Beachy, 1999; Oparka et al., 1996) direct replication proteins to the endoplasmic reticulum (ER). Within the family *Tombusviridae*, mitochondria and peroxisomes are the sites of replication (Burgyan et al., 1996; Rubino et al., 2001; Weber-Lotfi et al., 2002). While membrane association is possibly a universal feature of viral replication, in most cases, the mechanism of membrane targeting is unknown and there appears to be no correlation between virus phylogeny and the membrane systems recruited for replication.

Red clover necrotic mosaic virus (RCNMV) is a bipartite, positive-strand RNA virus in the *Dianthovirus* genus, *Tombusviridae* family (Fig. 1A; van Regenmortel et al., 1999). RNA-1 replicates independently of RNA-2 in protoplasts, but both RNAs are required for movement and plant infection (Osman and Buck, 1987; Paje-Manalo and Lommel, 1989; Sit et al., 1998; Xiong et al., 1993a). The RCNMV RNA-1 encodes two N-terminally overlapping proteins of 27 and 88 kDa (p27 and p88). p88 is generated via a −1 ribosomal frameshifting event from p27 and contains the "glycine-aspartate-aspartate" motif characteristic of RNA-dependent RNA polymerases (Kim and Lommel, 1994; Xiong et al., 1993b; Fig. 1A). Both p27 and p88 are highly conserved with the polymerases from other species in the *Tombusviridae* (Xiong and Lommel, 1989). While the role of p27 is unclear, it is very likely to be a component of the RCNMV replication complex because both p27 and p88 are immunoprecipitated from functional, template-dependent RNA polymerase preparations isolated from RCNMV-infected *Nicotiana clevelandii*

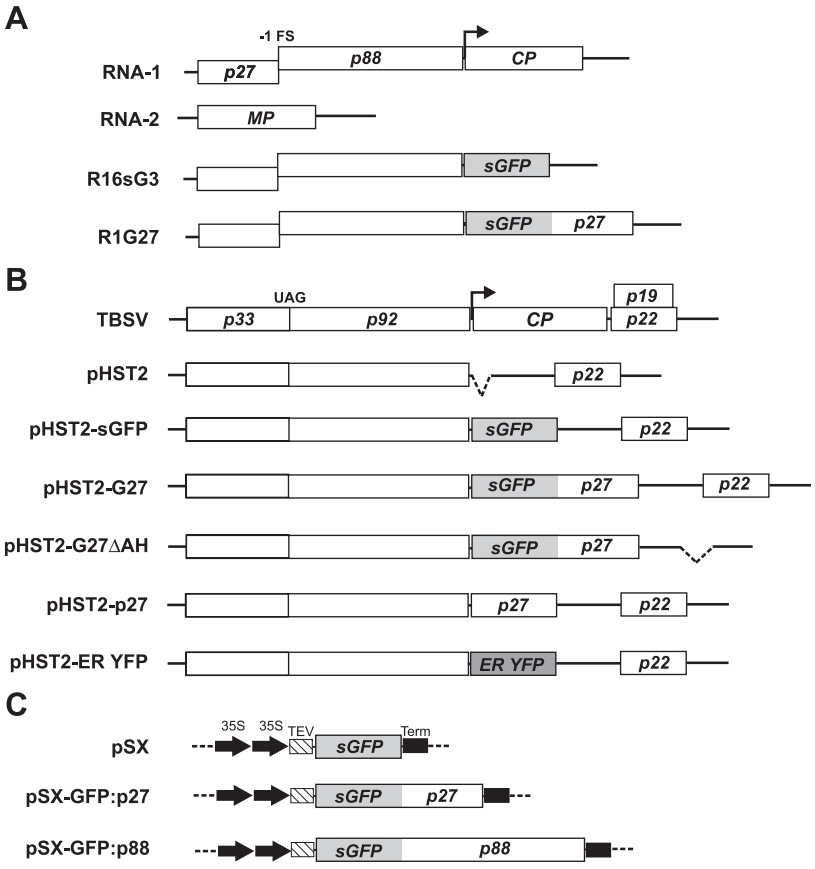

Fig. 1. Genome maps of RCNMV, TBSV, and various derivative p27- and p88-expression constructs. (A) Genomic RCNMV RNA-1 and RNA-2 along with RNA-1 derivatives R16sG3 and R1G27. Open reading frames (ORFs) for p27, the −1 ribosomal frameshift (−1 FS) product p88, capsid protein (CP), and movement protein (MP) are labeled. R16sG3 contains the coding region for GFP (shaded box) in place of the CP ORF. R1G27 produces a GFP:p27 translational fusion product in place of the CP. (B) Diagram of the TBSV genome, and constructs derived from the TBSV expression vector pHST2. The TBSV replication proteins (p33 and p92) along with the amber stop codon (UAG), CP, and pathogenicity or movement proteins (p19/p22) are labeled. In the pHST2 vector, a part of the CP ORF was removed and restriction sites were embedded to allow expression of foreign genes under the control of the CP subgenomic promoter (Scholthof et al., 1996). The dashed line denotes the deleted region. Additionally, the start codon for p19 has been deleted to prevent its expression. pHST2-sGFP expresses free GFP while pHST2-G27 produces a GFP:p27 fusion. pHST2-G27ΔAH contains a deletion in the p22 movement protein (denoted by a dashed line) that prevents movement out of the initially inoculated cell. pHST2-p27 expresses unlabelled p27. pHST2-ER YFP produces YFP (darker shaded box) with an ER-targeting signal sequence and cognate 'KDEL' retention signal. (C) pRTL2-based constructs for microprojectile bombardment and protoplast transfections. Dual Cauliflower mosaic virus 35S promoters (arrows labeled 35S), Tobacco etch virus leader sequence (hatched boxes labeled TEV), and NOS terminator (black boxes labeled Term) are depicted. pSX expresses free GFP. pSX-GFP:p27 expresses p27 fused to the 3′end of GFP. pSX-GFP:p88 expresses p88 as a 3′fusion to GFP.

(Bates et al., 1995). RNA-1 also encodes the viral capsid protein (CP) which is expressed from a subgenomic RNA (sgRNA; Sit et al., 1998; Zavriev et al., 1996). The CP is not required for replication or cell-to-cell movement (Xiong et al., 1993a).

To gain insight into the mechanisms of viral replication and pathogenesis, we investigated the localization of RCNMV polymerase proteins in plant cells using *Aequorea victoria* green fluorescent protein (GFP) fusions. Laser scanning confocal microscopy detected and identified the subcellular localization of fluorescent GFP:p27 and GFP:p88 fusions in real time and at high resolution. In this study, we demonstrate that RCNMV p27 and p88 localize to and accumulate at the ER and remodel the morphology of cortical and cytoplasmic ER domains.

Results

GFP:p27 expressed from RCNMV RNA-1 localizes to the ER

Transcripts from an RNA-1 cDNA clone with GFP fused to the amino terminus of the p27 open reading frame (ORF), and consequently also the p88 readthrough, were not infectious and were not further studied (data not shown). Furthermore, carboxyl-terminal fusions to p88 were not infectious on *Nicotiana benthamiana* or cowpea plants (Z. Xiong, personal communication). Because it appears that the polymerase does not tolerate heterologous protein fusions to either the amino- or carboxyl-termini, virus expression vectors based on RCNMV RNA-1 were constructed that expressed wild-type (wt) polymerase in addition to polymerase:GFP fusions from the CP cistron. p27 was inserted either 5′ or 3′ of the GFP ORF in construct R16sG3 (Fig. 1A) to produce p27:GFP or GFP:p27 fusions. Run-off transcripts from these linearized RNA-1 expression vectors are infectious and were co-inoculated with RCNMV RNA-2 transcripts onto *N. benthamiana* leaves. Resulting infections express wt levels of native p27 and much higher levels of GFP:p27, presumably at those approaching CP in an RCNMV infection.

Transcripts for constructs with a p27:GFP fusion were infectious but did not produce detectable fluorescence and were not further examined (data not shown). Clone R1G27, which contains a GFP:p27 fusion (Fig. 1A), generated an infection that moved cell-to-cell. The GFP:p27 fusion protein was expressed and accumulated stably in each infected cell. Fluorescence and confocal microscopy showed that the GFP:p27 localized and accumulated at or near the ER throughout the cell (Fig. 2A). Fluorescence from GFP:p27 was observed in a polygonal network of cortical ER (Figs. 2A and B, arrows) and several ER subdomains, including the nuclear envelope (Fig. 2A, small arrow). In addition, fluorescence was observed in large, amorphous aggregates that flowed along or within the tubular cytoplasmic ER (Fig. 2B, small arrow). The aggregates represented a distortion of normal ER structure (compare Fig. 3A to Figs. 2A and B), suggesting that the virus stimulated proliferation of ER cisternae (Carette et al., 2000; Rubino et al., 2000).

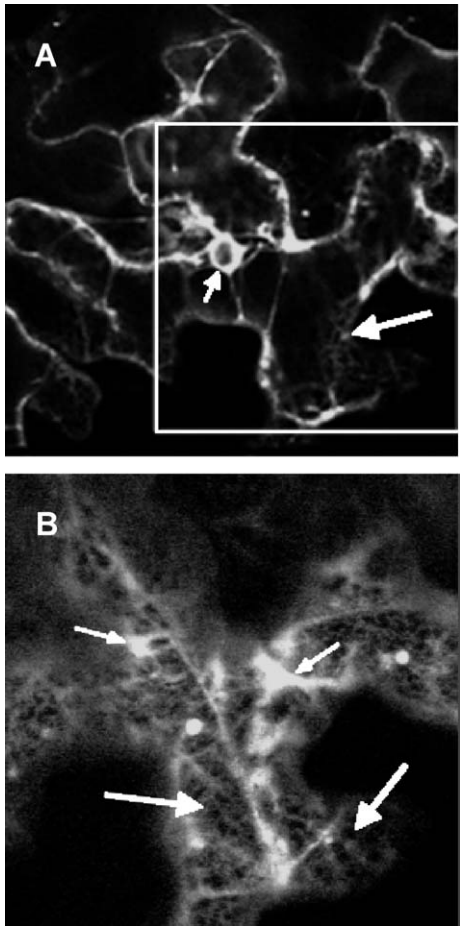

Fig. 2. Confocal micrographs of *N. benthamiana* epidermal cells after co-inoculation with R1G27 and RCNMV RNA-2 in vitro transcripts. (A) A computer projection of multiple optical sections showing both the cortical region and the central vacuole. The nuclear envelope (small arrow), transvacuolar strands, and cortical ER (large arrow) are shown. (B) An enlargement of the boxed area in panel A. Only the cortical region of a single optical section is shown to demonstrate the presence of cortical ER (large arrow), fluorescent aggregates (small arrow), and ER strands.

RCNMV rearranges ER morphology

Based on observations of R1G27 infections on *N. benthamiana*, transgenic plants expressing ER-localized GFP (GFP-ER *N. benthamiana*) were employed to determine the effect of RCNMV infections on ER morphology. In these plants, GFP is fused to an ER-targeting signal sequence and cognate ‘HDEL’ ER retention signal (Haseloff et al., 1997) and therefore localizes and accumulates in the ER where it fluoresces in the ER lumen and nuclear envelope (Fig. 3A).

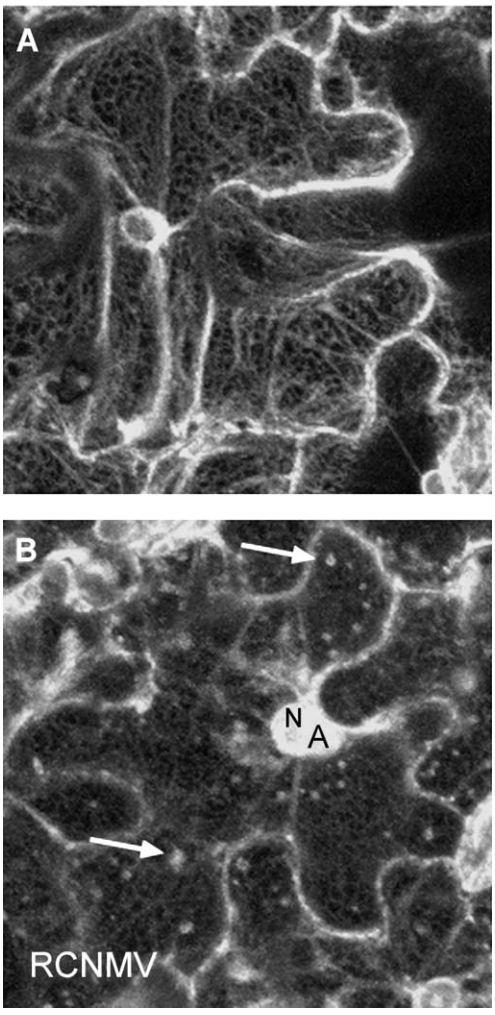

Fig. 3. Confocal images of transgenic *N. benthamiana* plants expressing GFP-ER. (A) Fluorescent ER structure of a mock-inoculated cell. (B) ER structure after wt RCNMV infection. The arrows show aggregates of ER membranes or fluorescent proteins. N = nucleus, A = aggregate.

A weblike, reticular network of relatively stationary, interconnected tubules is characteristic of the ER in the cortical region of plant and animal cells (Knebel et al., 1990; Staehelin, 1997; Terasaki and Reese, 1992). The GFP-ER *N. benthamiana* plants were inoculated with wt RCNMV infectious transcripts (RNA-1 and RNA-2) and observed by confocal laser scanning microscopy. RCNMV-infected cells exhibited fluorescence throughout the ER as expected. In addition, very large, perinuclear aggregates of fluorescence (Fig. 3B, labeled 'A') and many smaller aggregates in the region just underneath the plasma membrane, containing the cortical ER (Fig. 3B, arrows), were observed that were not seen in the absence of infection. The cortical ER was still detected, but its relative brightness, compared to mock-inoculated samples (Fig. 3A), was reduced. The smooth ER strands throughout the cytoplasm were thickened and proliferated (data not shown) compared to mock-inoculated samples.

p27 is associated with the ER membrane fraction

Cellular fractionation experiments were performed to biochemically verify the association of p27 with membranes. Equal weights of leaf tissue from mock-inoculated and RCNMV-infected *N. benthamiana* were homogenized and separated on sucrose gradients. The pellet and supernatant fractions were subjected to SDS-PAGE, transferred to Immobilon-P membranes (Millipore Corp., Bedford, MA), and subjected to analysis by Western blotting. p27 antisera and anti-BiP antisera were used to identify fractions containing those proteins. BiP is an ER-resident chaperonin (Terasaki and Reese, 1992; Wrobel et al., 1997) typically found in the supernatant fraction. No p27 signal was detectable in mock-inoculated tissue. In RCNMV-inoculated tissue, p27 predominantly fractionated with the supernatant with about 10–20% of the signal in the pellet (Fig. 4A). Detection in the pellet fraction was likely the result of some p27 associating with the nuclear envelope and dense protein aggregates. As expected, BiP was associated with the supernatant fraction containing cellular membranes in both mock- and RCNMV-inoculated tissues (Fig. 4B). Densitometry of the exposed films indicated that at least 20% more BiP signal was present in the RCNMV-inoculated tissue [compare Fig. 4B, Mock (T) to RCNMV (T)], suggesting that viral infection stimulates BiP production. Elevated levels of BiP suggest that the ER has proliferated or that increased levels of chaperonins are needed in response to viral infection.

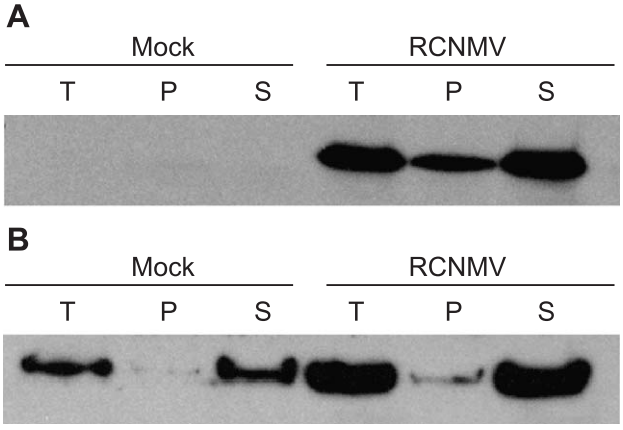

Fig. 4. Immunoblot analysis of RCNMV p27 and BiP proteins from *N. benthamiana* cellular fractionations. Mock- and RCNMV-inoculated plant tissues were homogenized in buffer A, applied to a 40–51% sucrose gradient, and centrifuged at 15000 × *g*. Total (T), pellet (P), and supernatant (S) fractions were separated by SDS-PAGE and visualized with anti-p27 or anti-BiP antisera. Cellular membranes remain in the supernatant. (A) Anti-p27 blot. p27 is found predominantly in the membrane fraction of RCNMV-inoculated tissue. A minor portion (less than 20%) remained in the pellet. No signal was detected in fractions from mock-inoculated tissue. (B) Anti-BiP blot. ER-resident binding protein (BiP) is found in the membrane fraction of mock- and RCNMV-inoculated tissue. Trace amounts were visualized in pellet fractions. The total amount of BiP present appears greater in RCNMV-inoculated plants (compare Mock (T) with RCNMV (T) in panel B).

Localization of GFP:p27 expressed from pHST2

A limitation of utilizing RCNMV RNA-1 for the expression of GFP:p27 is the presence of unlabelled p27. We cannot exclude the possibility that unlabelled p27 unduly influences the localization of the GFP:p27 fusion. To address this, a *Tomato bushy stunt virus* (TBSV) vector (pHST2; Scholthof et al., 1996) was employed to express the GFP:p27 fusion in the absence of any other RCNMV proteins. The GFP:p27 cassette from R1G27 was subcloned directly into the pHST2 vector to generate clone pHST2-G27 (Fig. 1B). In pHST2-G27, the GFP:p27 fusion is expressed from the TBSV CP subgenomic promoter. Two days after pHST2-G27 transcripts were inoculated to *N. benthamiana* leaves, hundreds of bright, fluorescent foci appeared. Similarly to GFP:p27 expressed from RCNMV RNA-1, the fluorescence was localized to the ER, specifically, the cortical (Fig. 5A) and perinuclear ER (Fig. 5B, large arrow) as well as thick cytoplasmic tubes of ER (Fig. 5B, arrowhead). Numerous small (ca. 1 μm), highly fluorescent bodies were also observed along the tubular ER and associated with the polygonal cortical ER network. The micron-sized bodies migrated rapidly along the ER tubules, often in a coordinated fashion. Additionally, they displayed saltatory movements, including reversing direction and stopping entirely for a brief time before resuming motion. Cells expressing GFP:p27 from pHST2-G27 maintained the reticular ER structure and cytoplasmic streaming, while displaying small aggregates of ER membranes.

To confirm the ER localization of GFP:p27 expressed from TBSV, confocal microscopy was used for co-localization experiments with an ER-targeted yellow fluorescent protein (YFP; Clontech, Palo Alto, CA) expressed from a second TBSV construct (pHST2-ER YFP; Fig. 1B). The YFP was modified by the addition of a calreticulin ER-targeting signal peptide and cognate 'KDEL' ER retention signal (Fliegel et al., 1989) to ensure its accumulation in the ER. For the co-localization experiments, pHST2-G27 was mutated to abolish cell-to-cell movement by partial deletion of the TBSV p22 movement protein (clone pHST2-G27ΔAH). Coinfections with the GFP and YFP clones could be identified by the presence of multicell foci expressing bright green fluorescence from GFP:p27 fusions that had movement complemented by the less fluorescent pHST2-ER YFP construct. In vitro transcripts of the pHST2-G27ΔAH and pHST2-ER YFP constructs were co-inoculated onto *N. benthamiana* leaves and the resultant foci were imaged. Although the spectra of GFP and YFP overlap considerably, microscope settings to minimize crosstalk among the fluorophores were used (see Materials and methods). In addition, the fluorophores were scanned independently to minimize crossover between the two channels. The resultant images were pseudo-colored green for the GFP:p27 signal and red for the ER YFP signal and digitally overlaid. Areas where the two signals overlapped appear yellow due to the mix of red and green pixels.

When spectroscopy was conducted on coinfected cells at 514 nm (green light), yellow fluorescence was observed from the YFP throughout the endomembrane system. The cortical ER was clearly visible (Fig. 5D, arrow) as were tubes of cytoplasmic ER (Fig. 5D, arrowheads). In all cases, the YFP was observed in the lumen of the nuclear envelope, which is contiguous with the lumen of the ER (Fig. 5C, arrow). Unexpectedly, the YFP was also observed within the nucleus. The ER targeting signal sequence in the YFP construct was derived from rabbit calreticulin (Fliegel et al., 1989). Although calreticulin is conserved throughout eukaryotes, in our viral-based expression system, it appears the mammalian signal peptide does not possess the same restriction in plants. When the same cells were observed under 488 nm (blue) light, green fluorescence from GFP was observed associated with the endomembrane system throughout the cell, in identical patterns to those described for pHST2-G27 (Fig. 5E). It could be clearly seen in the pseudo-color overlays of ER YFP and GFP:p27 that the fusion proteins co-localized, indicating that GFP:p27 accumulated predominantly within the cortical and tubular ER (Fig. 5D). In most coinfected cells, the interior of the nucleus exhibited red pseudo-color from the mistargeted ER YFP, while signal from both fluorophores was apparent within the nuclear envelope (Fig. 5C, arrow). GFP:p27 was seen within the nucleus in only one instance among the hundreds of imaged cells. It is not clear whether this was due to fluorescence associated with intranuclear ER tubules

Fig. 5. Confocal images of pHST2-G27, pHST2-G27ΔAH, and pHST2-ER YFP. In vitro transcripts of pHST2 constructs were manually inoculated to *N. benthamiana* leaves and imaged using confocal microscopy. Images represent computer projections of multiple confocal sections (at least 10 sections per cell, each section approximately 1 μm focal depth; panels A, C, and G–K) or individual 1 μm sections (panels B, D, E, and F). The boxed area in panel A represents the area enlarged in panels D–F. (A) Typical pattern of fluorescence produced after infection with pHST2-G27. (B) Interior section of similar cell showing characteristic ring around the nucleus (large arrow), cortical ER, and smooth ER tubules (arrowhead), as well as bright mobile spots (small arrows). (C) False color overlay of pHST2-G27ΔAH and pHST2-ER YFP. Both fluorophores are in the nuclear envelope (arrow). (D) pHST2-ER YFP in the cortical region. (E) pHST2-G27ΔAH and pHST2-ER YFP in the same cell showing the reticular, cortical ER, and punctate spots. (F) False color overlay of the two signals. GFP:p27 and ER YFP co-localize in the reticular network. (G–L) Transgenic *N. benthamiana* plants expressing GFP-ER. The fluorescence is exclusively from the ER-localized GFP. (G) Mock inoculation; represents unperturbed ER structure. (H) Inoculated with pHST2 vector. Aggregates (large arrow), thickened ER strands (small arrows), and perinuclear aggregates (arrowhead) are shown. (I) Inoculated with pHST2-p27. Thickened ER strands are shown (small arrows). (J) Inoculated with pHST2-ER YFP. The red circle indicates the nucleus. (K) Inoculated with wt RCNMV. Small aggregates (small arrows) and perinuclear aggregates (large arrow) are shown. The red circle indicates the nucleus. (L) Non-inoculated cell 4 h after incubation in 200 μg/ml brefeldin A. The loss of fluorescence in the cortical region and large blebs of membrane are characteristic of stressed, disrupted ER. Scale bars equal 10 μm.

(Collings et al., 2000) or a side effect of the mistargeted ER YFP.

TBSV alters ER morphology

Despite the absence of other RCNMV proteins, changes to the ER structure may not be a result exclusive to GFP:p27 expression. To examine the contribution of TBSV gene products to the observed ER modifications, control experiments were performed with each of the TBSV constructs inoculated onto GFP-ER *N. benthamiana* plants. In vitro transcripts of each construct were inoculated to GFP-ER transgenic plants and the ER was observed for changes by confocal microscopy. pHST2, the TBSV vector lacking

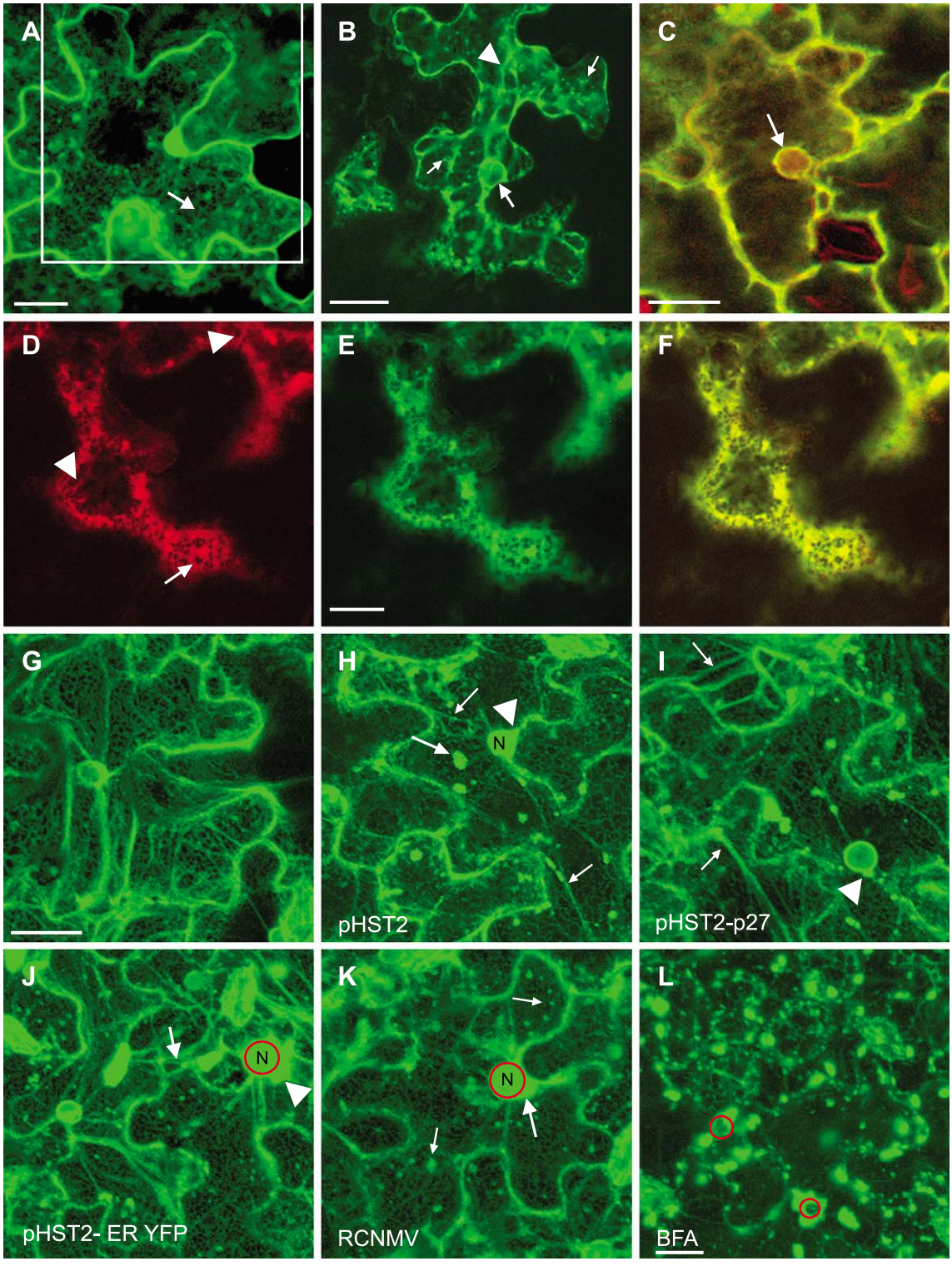

CP expression, induced ER aggregations in the cortical region (Fig. 5H, arrow) as well as thickening of the smooth ER strands that traverse the cell (Fig. 5H, small arrow). Some of the ER aggregates were in the perinuclear area (Fig. 5H, arrowhead). pHST2-p27 caused similar changes in ER structure, but to a slightly greater extent (Fig. 5I). The ER aggregates were larger and the smooth strands were thicker and more evident in the cortical region (Fig. 5I, small arrows), suggestive of ER membrane proliferation. The aggregates were also visible in the perinuclear region (Fig. 5I, arrowhead).

By comparison, the perinuclear aggregates were very large (Fig. 5K, large arrow), while the cortical aggregates were reduced in size and increased in number (Fig. 5K, small arrows) for GFP-ER *N. benthamiana* cells inoculated with wt RCNMV. The smooth ER strands were thickened and proliferated (Fig. 5K). The cytoplasmic aggregates observed in a wt RCNMV infection were not as large as those from TBSV-based infections, but the perinuclear aggregates were similar in size. Overall, the distortion of the ER in a wt RCNMV infection was less severe than that observed in a TBSV-based infection, a likely consequence of protein overexpression from pHST2.

In both RCNMV and TBSV construct inoculations, the reticular web of cortical ER in the GFP-ER *N. benthamiana* cells remained visible and relatively normal, with the aggregates and thickened strands superimposed upon it. Interestingly, in GFP-ER *N. benthamiana* cells inoculated with pHST2-ER YFP, large aggregates of ER formed in the perinuclear and cortical regions (Fig. 5J, arrowhead). Additionally, very small aggregates, similar to those seen with RCNMV, were observed (Fig. 5K). The cortical ER was not as evident in the cells, and the smooth ER strands were thickened and distorted (Fig. 5J, arrow). It was not immediately apparent why the presence of ER YFP would perturb the ER structure beyond the changes caused by the viral vector alone. For comparison, GFP-ER *N. benthamiana* leaves were infiltrated with brefeldin A, a fungal metabolite that disrupts the ER at concentrations of 100 μg/ml (Boevink et al., 1998). In treated leaves, the cortical ER was nearly absent and large aggregates of ER formed throughout the cell (Fig. 5L). This pattern of fluorescence is similar to that observed in GFP:p27-expressing cells.

Localization of GFP:p27 and GFP:p88 expressed from the CaMV 35S promoter

To observe the localization of and morphological changes induced by RCNMV p27, isolated from the effects of other cognate or heterologous viral proteins, GFP:p27 was cloned into the plant expression vector pRTL2 (Carrington et al., 1990). Clone pSX-GFP:p27 expresses a GFP:p27 fusion from the *Cauliflower mosaic virus* (CaMV) 35S promoter (Fig. 1C). The DNA-based pRTL2 vector also allowed for the stable expression of a GFP:p88 fusion protein from construct pSX-GFP:p88. Previous attempts to stably express GFP:p88 in either RCNMV RNA-1 or pHST2 were unsuccessful (data not shown). In pSX-GFP:p88, the frameshift signal was abolished, allowing expression of an uninterrupted ORF for the 88-kDa protein. This facilitated the localization of the core p88 polymerase subunit independently of p27.

Localization of GFP:p27 and GFP:p88 expressed in epidermal cells

Plasmids pSX-GFP:p27 and pSX-GFP:p88 were microprojectile bombarded (Sanford et al., 1993) into detached *N. benthamiana* leaves. Epidermal cells were examined 24 h after bombardment by confocal microscopy. In cells bombarded with pSX-GFP:p27, fluorescence was associated with the ER throughout the cell (Figs. 6A–D). Fluorescence was seen in the cortical ER (Figs. 6 A, B, and D, arrows) as well as in the nuclear envelope (Figs. 6B and C, arrowhead) in patterns nearly identical to those observed in R1G27-inoculated cells. However, the cortical ER of the bombarded cells appeared to be brighter than the ER of R1G27-inoculated cells.

In addition to regular endomembrane patterns, fluorescence was also seen in large aggregates of membranes or proteins (Figs. 6A, C, and D, labeled ‘A’) and numerous small, motile bodies (Fig. 6B, open arrow), which flowed along or in the tubules of ER. It was often possible to see strands or tubes of fluorescent material within the nucleus (Fig. 6D, open arrowhead). In all cases, the fluorescence patterns observed were distinct from the diffuse cytoplasmic fluorescence observed in cells bombarded with pSX expressing GFP alone (Fig. 6I). The ER fluorescence pattern observed in cells bombarded with pSX-GFP:p27 was identical or nearly identical to that observed in RCNMV-inoculated GFP-ER *N. benthamiana* plants or epidermal cells infected with R1G27 (compare Figs. 6A–D with Figs. 2B and 3B).

The GFP:p88 fusion protein was also associated with the endomembrane system throughout the cell. Fluorescence was detected in the reticular network of the cortical ER (Figs. 6E and F, arrows), in smooth ER tubules bundled along the actin cytoskeleton (as described by Staehelin, 1997) (Fig. 6F, star), and in large membrane or protein aggregates (Figs. 6E and G, labeled ‘A’). Some cells also exhibited apparent nuclear localization of GFP:p88 (Fig. 6G, open arrowhead). There are no identifiable nuclear targeting motifs in either p27 or p88, and the GFP:p88 fusion protein is ca. 115 kDa, far too large to passively diffuse into the nucleus. In some cells expressing GFP:p88, the characteristic polygonal pattern of the ER appeared diffuse and faint, resembling the cytoplasmic distribution of fluorescence in cells expressing free GFP (compare Figs. 6H and I). This appearance is particularly pronounced in computer projections of multiple optical sections of leaf epidermal cells. Overall, the number of

expressing cells and amount of fluorescence produced by pSX-GFP:p88 in epidermal cells were very low compared to the expression of free GFP controls. To more efficiently identify cells expressing GFP:p88 and GFP:p27, the various pSX constructs were transfected into *N. benthamiana* protoplasts.

Localization of fusion proteins expressed in protoplasts

Twenty-four hours after inoculation with pSX-GFP:p27, fluorescence was observed in punctate spots throughout the protoplast cytoplasm (Fig. 7B). The puncta were connected by a network of finely stretched membranes, suggesting that they were derived from ER or contained within it (Fig. 7B, arrows). This fluorescence pattern strongly resembles the early stages of ER disruption by brefeldin A (Ritzenthaler et al., 2002; see Fig. 5L) and is noticeably different from the distribution of free GFP (Fig. 7A).

Fluorescence generated from the pSX-GFP:p88 fusion protein was detected throughout the cytoplasm and appeared to localize to the nucleus (Fig. 7C). In addition, fluorescent aggregates associated with the endomembrane system in a pattern similar to that seen for GFP:p27 expressed from pSX-GFP:p27 (data not shown). Approximately 22% (62/283) of the cells expressing GFP:p88 exhibited fluorescent punctate spots, with the remainder showing diffuse fluorescence. In approximately 75% of the cells, the fluorescent protein appeared to occupy the entire cytoplasmic volume of the cell, making subcellular structural observations impossible.

In protoplasts inoculated with both pSX-GFP:p27 and pSX-GFP:p88, fluorescence was observed in aggregates throughout the endomembrane system, which was swollen and distorted (Fig. 7D). In addition, fluorescence could be detected from within the nucleus, in cytoplasmic strands, and aggregates (Figs. 7D, arrow, E, and F). It has been demonstrated that the ER forms grooves and tunnels throughout the nucleus in plant cells (Collings et al., 2000) including *N. benthamiana*, suggesting that the fluorescence observed in the nucleus is actually GFP:p88 and GFP:p27 localized to the ER that is in close contact or extends through the nucleus. In all cases, the percentage of protoplasts that survived inoculation with the

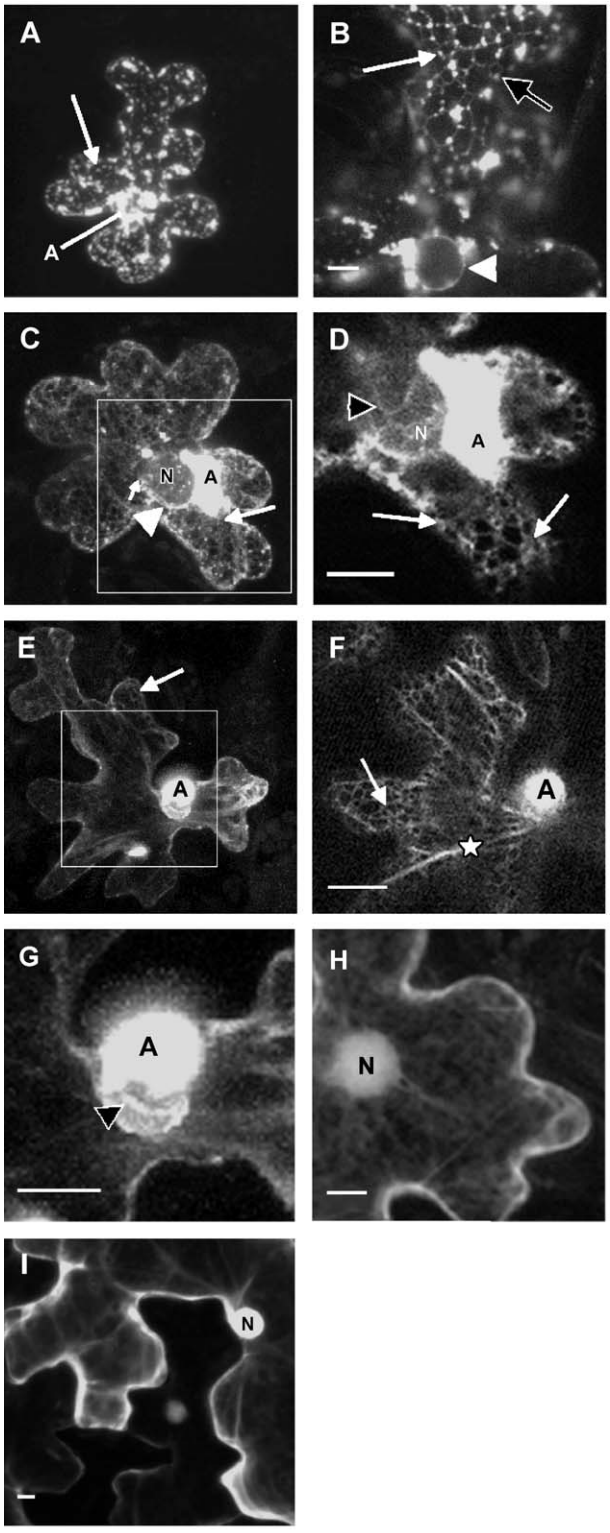

Fig. 6. Confocal images of GFP:p27 and GFP:p88 accumulating in the ER of microprojectile bombarded *N. benthamiana* epidermal cells. Images represent computer projections of multiple confocal sections (at least 10 sections per cell, each section approximately 1 μm focal depth; panels A, C, E, and G–I) or individual 1 μm sections of the same cells to the left (panels B, D, and F). The boxes indicate which region of the cell is enlarged. (A–D) Cells bombarded with pSX-GFP:p27. (A and B) Cortical ER (arrows), intensely fluorescent motile bodies (open arrow), and nuclear envelope (arrowhead) are observed. (C and D) Fluorescent aggregates and tubules through the nucleus (open arrowhead) can be seen. (E–H) Cells bombarded with pSX-GFP:p88. (E) Large fluorescent aggregate ("A") and reticular ER (arrows) are denoted. (F) Enlarged cortical section view of cell presented in panel E showing the thick ER strands (star). (G) Enlarged view of the same nucleus shown in panels E and F, highlighting the ER strands through the nucleus (open arrowhead). (H) GFP:p88 displaying the diffuse fluorescence pattern. (I) Free GFP in epidermal cells. N = nucleus. Scale bars equal 10 μm.

RCNMV fusions was low, and the cells often appeared to be in the early phases of apoptosis. The fluorescence output per cell was also low compared with free GFP controls.

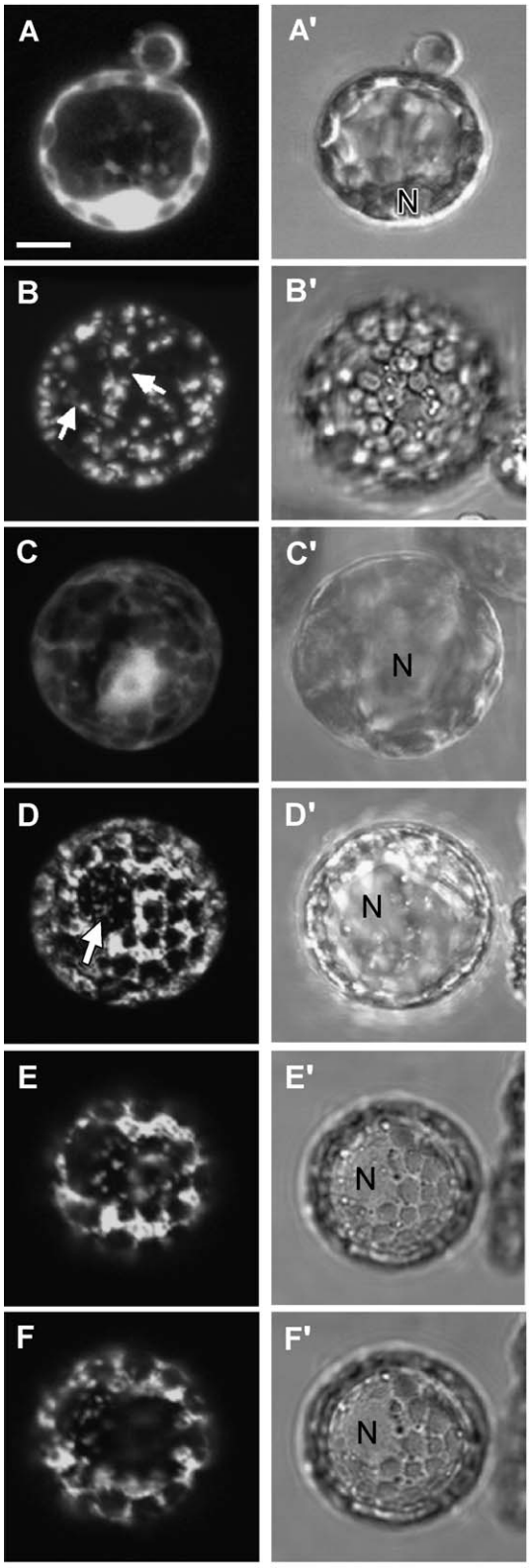

Discussion

Eukaryotic positive-stranded RNA viruses replicate in association with intracellular membranes. This is true for both plant and animal viruses, even for those that are non-enveloped and do not use glyco- or phospholipids for assembly or transmission (Ahlquist et al., 1994; Schlegel et al., 1996; Schwartz et al., 2002, and references therein). In this study, we investigated the intracellular localization of the RCNMV p27 and p88 replication proteins. RCNMV caused morphological changes in the ER of GFP-ER transgenic plants. These changes included thickening of ER tubules and formation of large fluorescent aggregates near the nuclei (Fig. 3B). Because the distortion of ER increases over time in RCNMV-inoculated cells, it is likely that the ER membranes are undergoing active restructuring due to the presence of the virus and accumulation of viral gene products. p27 was found primarily in membrane fractions of infected *N. benthamiana* leaves, and RCNMV-infected cells displayed elevated levels of BiP, consistent with ER proliferation and pathology (Fig. 4). In poliovirus studies, electron micrographs revealed direct budding of poliovirus-induced membranes from rough ER and brefeldin A treatment inhibited poliovirus RNA replication, strongly suggesting that the ER is the source of poliovirus-induced membranes. However, cellular markers for the ER, Golgi, and lysosomes are equally represented in membranous structures (Schlegel et al., 1996). These contradictory observations could indicate that virus infection perturbs the lipid balance of the entire secretory pathway or even of the whole cell. It has been shown that some RNA viruses require a specific lipid environment for replication (Bong et al., 1999; Carette et al., 2000; Lee et al., 2001).

In epidermal cells and protoplasts, the fluorescence of GFP:p27 displayed two distinct localization patterns. The weblike cortical ER can clearly be delineated in most cells despite distortion to normal ER morphology. This distortion may be due to the induced proliferation of ER membranes by GFP:p27. Additional large fluorescent aggregates along with

Fig. 7. Confocal images of PEG-inoculated *N. benthamiana* protoplasts transfected with pSX, pSX-GFP:p27, pSX-GFP:p88, or pSX-GFP:p27 + pSX-GFP:p88. Fluorescence was observed via confocal microscopy 24 h after transfection. (A–D) Computer projections of multiple confocal sections. (A′–D′) Corresponding DIC-transmitted light micrographs of the cells. (E and F) GFP:p27 + GFP:p88 single 1 μm confocal section. (E′and F′) Corresponding DIC micrographs (A) pSX characteristic diffuse fluorescence throughout the cytoplasm and nucleus. The large central vacuole does not contain GFP. (B) pSX-GFP:p27 protein aggregates and fine membranes stretched between them. (C) pSX-GFP:p88 fluorescence appears to fill the volume of the cell. The dark circular patches represent where GFP:p88 is excluded from the chloroplasts. (D) pSX-GFP:p27 and pSX-GFP:p88 fluorescence fill the entire volume of the cell, distorting the ER membranes. Fluorescent aggregates are within the nucleus. (E and F) pSX-GFP:p27 and pSX-GFP:p88. Individual 1-μm sections demonstrate that the fluorescent aggregates occur in the area bounded by the nuclear membrane and are not simply visible "through" the nucleus as an artifact of confocal imaging. Scale bar equals 10 μm.

tiny, motile, fluorescent bodies were observed in other cells. The large aggregates likely represent centers of viral replication called multivesicular bodies in tombusvirus infections (Burgyan et al., 1996), while the smaller aggregates may represent Golgi bodies (Boevink et al., 1998) or an undefined ER subdomain.

To verify the ER localization of GFP:p27, a co-inoculation experiment was performed. GFP:p27 co-localized with the ER-targeted YFP in the cortical and cytoplasmic ER. Unexpectedly, the ER YFP was also visualized in the interior of the nucleus in all fluorescent cells. The rabbit-derived ER-targeting signal sequence was likely not able to direct the YFP solely to the ER in plant cells, or the presence of replicating TBSV in the cell may have disturbed the ER to such an extent that contents from the ER lumen were misdirected into the nucleus. Because GFP:p27 generally stayed within the nuclear envelope, while ER YFP escaped (Fig. 5C), it is more likely that the signal targeting sequence was not restrictive enough in the ER YFP system. This may simply be a result of variation in the strength and degree of specificity between GFP:p27 and ER YFP for ER localization. However, this difference also raises interesting questions about the mechanisms of protein targeting in plants versus animals. If the Golgi targeting sequence from rat sialyltransferase localizes GFP to the plant Golgi unambiguously (Horsley et al., 1993; Wee et al., 1998), despite dramatic differences in Golgi morphology and behavior between plant and animal cells (Nebenführ et al., 1999), why doesn't the ER targeting signal perform similarly? For the future, it will be important to determine what other cellular systems are different between plants and animals, and how these differences impact protein targeting. In the meantime, it is important to consider the origin of targeting sequences when designing localization experiments. Although the ER YFP construct displayed nuclear localization in addition to the expected cortical and smooth ER localization, it is still a useful visible marker for ER in the cell. The fact that GFP:p27 co-localized extensively with ER YFP in co-inoculated cells, except for the interior of the nucleus which was devoid of detectable p27 fusion protein (except for one instance), supports the hypothesis that the RCNMV polymerase accumulates at the ER in virus-infected plants.

To observe the inadvertent effects of TBSV vector proteins on ER morphology, transgenic plants expressing GFP-ER were inoculated with TBSV-based viral constructs and wt RCNMV. TBSV and RCNMV are phylogenetically related and share sequence conservation in the polymerase proteins. TBSV is associated with membrane fractions in virus-infected plants but not specifically with the ER (Scholthof et al., 1995). Other tombusviruses have been previously shown to associate with peroxisomal or mitochondrial membranes (Burgyan et al., 1996; Rubino and Russo, 1998). All of the constructs tested perturbed the ER to some degree, including the TBSV vector alone. This fact modulates our interpretation of the experiments using this vector, as effects of the RCNMV proteins must be observed in a background of effects from the TBSV vector. The ER in wt RCNMV-inoculated GFP-ER plants was similar in appearance to the fluorescence patterns in GFP:p27-expressing cells. The fact that wt RCNMV caused perinuclear aggregates and small cytoplasmic aggregates in GFP-ER plants indicates that some of the ER distortion observed in pHST2-G27 (expressing GFP:p27)-inoculated plants is due to the presence of p27. However, we cannot quantify the level of distortion attributable to RCNMV. It is clear that RCNMV p27 localizes to the ER. The evidence is persuasive, regardless of the perturbation to normal ER structure due to the vector. This is a confirmation that the ER localization observed in those experiments represents a biologically relevant part of the natural RCNMV replication cycle, and not an artifact of protein overexpression, GFP expression, or spurious localization. It is important to emphasize that while TBSV is related to RCNMV and appears to have a mild effect on ER structure, in this investigation, it was used only as a vector and its relationship to RCNMV is incidental.

The fluorescence pattern of overexpressed GFP:p88 was variable and included the web of cortical ER, large aggregates, and diffuse fluorescence that could not be unambiguously attributed to any organelle. The variation in fluorescence patterns for GFP:p27 and GFP:p88 along with the diffuse fluorescence pattern seen in the majority of GFP:p88-inoculated cells is likely due to degradation of the normal, reticular ER structure and may be indicative of general membrane reorganization in the cell. In keeping with this, the aggregate patterns in GFP:p27 and GFP:p88 expressing cells resembled the morphology of ER that has been disrupted by brefeldin A (Fig. 5L) and may be the early stages of apoptosis in overexpressing cells. Alternatively, p88 may localize to the ER in viral infections through an interaction with p27 or some other viral protein. This is supported by the observation that GFP:p27 appears to change the localization pattern of GFP:p88 from diffuse with large aggregates (Fig. 7C) to one resembling GFP:p27 alone (compare Figs. 7B and D).

Tubular projections and aggregates of fluorescence were observed within the nuclei of GFP:p27- and GFP:p88-expressing cells and protoplasts. Collings et al. (2000) demonstrated that plant nuclei have extensive grooves and invaginations that are contiguous with the ER membranes. These tubes ramify throughout the nucleus of plant and animal cells (Collings et al., 2000; Fricker et al., 1997). Such an intimate connection between the nuclear interior and the ER could provide increased surface area for translation or could provide isolated domains for assembly of protein complexes destined to be transported by the secretory pathway (Fricker et al., 1997; Lui et al., 1998). It is consistent with this observation that fluorescence from GFP:p27 and GFP:p88 could be associated with the ER while appearing to be inside the nucleus.

GFP:p27 and GFP:p88 independently localize to the ER causing morphological changes (Fig. 6). Additionally, GFP:p27 co-localized with GFP:p88 to the ER of inoculated

N. benthamiana protoplasts (Fig. 7), suggesting that both proteins work to establish a replication site within the cell. Because GFP:p27 and GFP:p88 independently localized to the ER, both the pre- and post-readthrough portions must share an N-terminal localization domain or have distinct ER targeting properties. It has been hypothesized that one component of bipartite viral polymerases functions as a membrane anchor, while the other components assemble the holoenzyme around the anchor (Schaad et al., 1997). RCNMV may be a case of a replication complex that assembles without a specific anchor, each component associating with membranes or other components through hydrophobic interactions.

Each of the methods for the expression of GFP:p27 has revealed new information about its localization. It is possible that the localization of p27 changes over the course of time in response to undiscovered factors. Multifunctional proteins often have multiple localizations (Kong and Hanley-Bowdoin, 2002). It has been observed that TBSV replication p33 and p92 proteins accumulate in membrane fractions isolated from protoplasts early in infection and accumulate in the cytoplasmic fraction later in infection, before collapse of the tissues (Scholthof et al., 1995). It has also been reported that viral replication proteins can have multiple localizations correlated with time after infection. The TMV 126/183 kDa polymerase proteins co-localize with ER during the early stages of an infection, move from the ER to microtubules during the middle stages, and later traffic along them to the plasmodesmata (Mas and Beachy, 1999). The variation in RCNMV p27/p88 localizations may be due to differing roles during the infection cycle as well.

GFP:p27 localizes to the ER when expressed from three different promoters, in the presence of heterologous and homologous viral genomes, as well as in the absence of any other viral proteins. GFP:p88 co-localizes with GFP:p27 in protoplasts. Taken together, these observations suggest that the two proteins co-localize to the cortical ER, the nuclear envelope, and tubular cytoplasmic ER domains. The RCNMV polymerase components do not complement replication when expressed in *trans* from separate RNAs (Kim, 1993). It is therefore impossible to directly observe the individual-labeled proteins in a functional replication complex. When expressed individually, both p27 and p88 accumulate in the ER and perturb the ER morphology, suggesting that the proteins function together to establish a replication complex. Such a complex likely contains host proteins in addition to those of RCNMV (Bastin and Hall, 1976; Lee et al., 2001; Schwartz et al., 2002).

Materials and methods

Construction of clones

RCNMV p27 and p88 GFP fusions were expressed directly from an RCNMV RNA-1 infectious cDNA clone (RC169), a heterologous TBSV viral vector (pHST2), or a transient DNA plant expression vector (pRTL2). All constructs were verified by restriction digestion or sequence analysis.

An RCNMV RNA-1 cDNA construct was first engineered to express a synthetic copy of GFP (GFP; Chiu et al., 1996) in place of the CP ORF that allows the production of either amino- or carboxyl-terminal fusions to GFP (Fig. 1A). The GFP was amplified by PCR with *PfuTurbo* DNA polymerase (Stratagene, La Jolla, CA) using plasmid blue-SGFP-TYG-nos KS as the template and primers sGFP 5′ 6XHIS and sGFP 3′ΔNM (see Table 1). The DNA fragment was cleaved with *Cla*I/*Mlu*I and ligated into similarly cleaved RC169 to generate clone R16sG3. RCNMV p27 was amplified using RC169 as the template with primers p27-5′ *Cla*I/*Nco*I and p27-3′ *Xho*I/*Mlu*I (Table 1). The resultant PCR product was digested with *Nco*I/*Mlu*I and inserted into R16sG3 to produce clone R1G27 that expresses a GFP:p27 fusion protein.

The TBSV vector pHST2 was previously engineered to allow expression of foreign sequences from the CP subgenomic promoter (Fig. 1B; Scholthof et al., 1996). The GFP

Table 1
Primers used in PCR reactions

Primer name	Sequence 5′ to 3′
sGFP 5′6XHIS	GTCCATGGGATCGATGCATCATCATCATCATCATGTGAGCAAGGGCGAGGAGCTG
sGFP 3′ΔNM	GTACGCGTCCATGGCCTTGTACAGCTCGTCCATGC
p27-5′ *Cla*I/*Nco*I	CTATCGATGGCCATGGGTTTTATAAATCTTTCGC
p27-3′ *Xho*I/*Mlu*I	GCACGCGTCTCGAGCTAAAAATCCTCAAGGGATTTG
p27-5′ERV/SNABI	GCAGATATCTACGTACCAGTCATGGGTTTTATAAATCTTTCGC
ER YFP 5′ *Sna*/*Xho*	TAGCTATACGTACTCGAGATGCTGCTATCCGTGCCGTT
ER YFP 3′ *Sca*/*Xba*	CTAGAGCTCTCTAGATTACAGCTCGTCCTTCTTGTACAG
sGFP 3′MKSX	GCATTCTAGATTAACTAGTCATGGTACCACGCGTCTTGT
p88-5′ *Mlu*/*Kpn*	GATACGCGTGGTACCATGGGTTTTATAAATCTTTCGCTT
p27-3′ *Xba*/*Bam*	CTAGGGATCCTCTAGACTAAAATCCTCAAGGGATTTGAAC
FpRC169p88	CTAGGCGGCCCACTCAGCTTTCCGGTT
RpRC169p88	GAAATCCTCAAGGGATTTGAACCCGGCAACA
p88-3′ *Not*/*Spe*	TAAACTATACTAGTGCGGCCGCTTATCGGGCTTTGATTA

ORF from R16sG3 was inserted into pHST2 with *Bgl*II/*Mlu*I to generate construct pHST2-sGFP (Fig. 1B). The GFP:p27 cassette from clone R1G27 was digested with *Cla*I/*Mlu*I and cloned into similarly digested pHST2-sGFP to produce construct pHST2-G27 (Fig. 1B). A movement-defective version of pHST2-G27 was produced by digestion with *Age*I/*Hpa*I to remove a 422-bp fragment, followed by blunt-ending with Klenow and religation. The resultant clone, pHST2-G27ΔAH (Fig. 1B), does not produce a functional p22 movement protein. A pHST2 construct expressing p27 alone was also produced by PCR using RC169 as the template for p27 and primers p27-5′ERV/SNABI and p27-3′ *Xho*I/*Mlu*I (see Table 1). The resultant fragment was cleaved with *SnaBI*/*Xho*I and ligated into similarly cleaved pHST2 to yield clone pHST2-p27 (Fig. 1B).

A control pHST2 construct for co-localization experiments was produced that expresses an ER-targeted yellow fluorescent protein (ER-YFP). The ER-YFP sequence was amplified from plasmid pEYFP-ER Vector (Clontech) using primers ER YFP 5′ *Sna*/*Xho* and ER YFP 3′ *Sac*/*Xba* (Table 1). The resultant fragment was digested with *Xho*I/*Sac*I and ligated into similarly cleaved pHST2 to generate pHST2-ER YFP (Fig. 1B).

A DNA-based plant expression vector pRTL2 (Carrington et al., 1990) was also used to express GFP fusions from the CaMV 35S promoter. GFP was amplified from plasmid blue-SGFP-TYG-nos KS as the template with primers sGFP 5′ 6XHIS and sGFP 3′ MKSX (Table 1), digested with *Nco*I/*Xba*I, and ligated to similarly cleaved pRTL2 to produce plasmid pSX (Fig. 1C). p27 was amplified with primers p88-5′*Mlu*/*Kpn* and p27-3′ *Xba*/*Bam* (Table 1), digested with *Mlu*I/*Xba*I, and ligated to similarly cleaved pSX to produce pSX-GFP:p27 (Fig. 1C).

Before generation of GFP:p88 fusion constructs, the p27 stop codon at the −1 ribosomal frameshifting site within p88 was altered to a leucine residue. This was accomplished via site-directed mutagenesis of RCNMV RNA-1 clone RC169 using an inverse long PCR method (Callaway, 1998). Mutagenesis was performed with primers FpRC169p88 and RpRC169p88 (Table 1) to generate mutant RC169-p88 that expresses only the 88-kDa protein from the N-terminal ORF. Subsequently, p88 was amplified from RC169-p88 by PCR with primers p88-5′*Mlu*/*Kpn* and p88-3′ *Not*/*Spe* (Table 1), digested with *Mlu*I/*Spe*I, and ligated to similarly cleaved pSX to produce pSX-GFP:p88 (Fig. 1B).

Plant inoculations with RNA transcripts

RCNMV and TBSV RNAs were transcribed from *Sma*I-linearized templates with T7 RNA polymerase (Pokrovskaya and Gurevich, 1994). RNA in 10 mM phosphate buffer was used to inoculate four leaves of carborundum-dusted *N. benthamiana* plants at the six- to eight-leaf stage. The plants were kept in a glasshouse at 21 °C. Each construct was inoculated to two plants and each experiment was repeated at least three times.

Microprojectile bombardment of detached leaves

Gold particles (1 μm; Bio-Rad, Hercules, CA) were coated with pSX, pSX-GFP:p27, or pSX-GFP:p88 plasmid DNA alone or in combinations, following the manufacturer's directions. Particles were delivered into *N. benthamiana* epidermal cells on detached leaves using the Biolistic PDS-1000/He system (Bio-Rad) with 1100 psi rupture disks under vacuum of 27 in. of Hg. After bombardment, the cut petioles were wrapped with dampened Kimwipes (Kimberly-Clark Corp., Roswell, GA) and sealed in plastic Petri dishes. Leaves were incubated at room temperature overnight before being imaged via fluorescence microscopy.

Protoplast inoculations

Protoplasts were prepared from either young *N. benthamiana* plants or a *N. benthamiana* suspension cell culture and inoculated essentially as described in Negrutiu et al. (1987), with modifications described in Brough et al. (1992). Briefly, after preparation, the protoplasts were inoculated with 5 μg of DNA in the presence of PEG 4000 (Sigma-Aldrich, St. Louis, MO) to permeabilize the membranes, washed with buffer, and allowed to recover overnight before being imaged by fluorescence microscopy.

Live cell microscopy

Plant cells were observed and selected for further confocal observation using a Zeiss Axiopohot epifluorescence microscope (Carl Zeiss, Oberkochen, Baden-Wuerttemberg, Germany) equipped with a long-pass FITC filter set. Confocal microscopy was carried out on a Leica DMIRBE inverted microscope (Leica Microsystems AG, Wetzlar, Germany) equipped with a spectral scanning head and a 63 × 1.2 NA water-immersion lens and transmitted light Differential Interference Contrast (DIC) capability. An argon laser (488 and 514 nm lines) was used to discriminate between the GFP and YFP fluorophores. In experiments where both fluorophores were analyzed, the emission signal from GFP was collected via photomultiplier tube from 500 to 515 nm and the emission from YFP was collected from 530 to 565 nm. In single-label experiments, the signal from GFP was collected from ca. 500 to 565 nm. The GFP channel was assigned false green and the YFP channel false red color. Images were processed using Photoshop 4.0 software (Adobe Systems, Mountain View, CA) and overlaid using MetaMorph software (Universal Imaging Corp., Downingtown, PA).

Membrane fractionation

Equal weights of mock- or wt RCNMV-inoculated *N. benthamiana* leaves were ground in buffer A (50 mM Tris–HCl pH 7.4, 15 mM $MgCl_2$, 10 mM KCl, 0.1% β-mercaptoethanol, 1 μm pepstatin, 0.1 mM PMSF, 20% glycerol)

using a mortar and pestle. The slurries were filtered through cheesecloth and equal volumes of the filtrates were applied to sucrose density gradients ranging from 40% to 51% sucrose. The plant and viral proteins were sedimented by centrifugation at 15000 × *g* in a tabletop microfuge. The membrane fraction floating on top of the 40% sucrose fraction (the "supernatant") was identified by the bright green color due to the presence of chloroplast membranes. The pellet at the bottom of the tube contained cell debris, nuclei, and heavier plastids (den Boon et al., 2001). Volumes equivalent to the volume of applied homogenate were collected from the pellet and supernatant for Western blot analysis.

Western blots

Protein extracts from ground leaves were prepared as described by Petty et al. (1989) and quantified using the Bradford Assay (Bio-Rad). Samples of the leaf extracts were applied to either 15% acrylamide handcast or 12.5% acrylamide precast (Bio-Rad) SDS-PAGE gels and separated and transferred as described by Vaewhongs and Lommel (1995). p27 was detected using a polyclonal anti-p27 antibody (Xiong et al., 1993b). BiP was detected using a polyclonal anti-BiP antibody (Fontes et al., 1991). Primary antibodies were detected with alkaline phosphatase-conjugated secondary antibodies (Bio-Rad), and the labeled proteins were visualized using the CDP-Star chemiluminescence kit (Novagen, Madison, WI) as directed by the manufacturer, and exposed to Kodak BioMax MS film.

Densitometry

The exposed films were quantified using ImageQuant Mac software version 1.2 (Amersham Biosciences Corp., Piscataway, NJ) with constant areas selected between bands and background subtraction performed by the software.

Acknowledgments

We thank J. Sheen for the GFP plasmid, J. Carrington for the pRTL2 vector, H. Scholthof for the pHST2 vector, D. Baulcombe for the ER-localized GFP transgenic *N. benthamiana*, and L. Hanley-Bowdoin for the *N. benthamiana* suspension cell culture. We thank D.A. Collings for assistance with microscopy, E. Johannes for advice on protoplasts and confocal microscopy, and Mara Massel for helpful discussion. Thanks especially to K. Nielsen for help with Western blots, R.S. Boston for anti-BiP, and Kirk Francis for help with protein quantification. This work was supported by a NSF/DOE/USDA training Grant # 546142-06284 to S.A.L. and K.A.T., USDA NRI competitive grant 98-02298 to S.A.L. and T.L.S., NSF competitive grants MCB-0077964 to S.A.L. and T.L.S, and NASA competitive grant NAGW-4984 to N.S.A.

References

Ahlquist, P., Wu, S.X., Kaesberg, P., Kao, C.C., Quadt, R., DeJong, W., Hershberger, R., 1994. Protein–protein interactions and glycerophospholipids in bromovirus and nodavirus RNA replication. Arch. Virol., Suppl. 9, 135–145.

Bastin, M., Hall, T.C., 1976. Interaction of elongation factor 1 with aminoacylated brome mosaic virus and tRNAs. J. Virol. 20, 117–122.

Bates, H.J., Farjah, M., Osman, T.A.M., Buck, K.W., 1995. Isolation and characterization of an RNA-dependent RNA polymerase from *Nicotiana clevelandii* plants infected with red clover necrotic mosaic dianthovirus. J. Gen. Virol. 76, 1483–1491.

Boevink, P., Oparka, K., Santa Cruz, S., Martin, B., Betteridge, A., Hawes, C., 1998. Stacks on tracks: the plant Golgi apparatus traffics on an actin/ER network. Plant J. 15, 441–447.

Bong, D.T., Steinem, C., Janshoff, A., Johnson, J.E., Reza Ghadiri, M., 1999. A highly membrane-active peptide in Flock House virus: implications for the mechanism of nodavirus infection. Chem. Biol. 6, 473–481.

Brough, C.L., Sunter, G., Gardiner, W.E., Bisaro, D.M., 1992. Kinetics of tomato golden mosaic virus DNA replication and coat protein promoter activity in *Nicotiana tabacum* protoplasts. Virology 187, 1–9.

Burgyan, J., Rubino, L., Russo, M., 1996. The 5′-terminal region of a tombusvirus genome determines the origin of multivesicular bodies. J. Gen. Virol. 77, 1967–1974.

Callaway, A.S., 1998 (Ph.D). A Genetic Approach to Study Host Factors of *Arabidopsis thaliana* that Influence Susceptibility to Cauliflower Mosaic Virus. Cornell University, Ithaca, NY.

Carette, J.E., Stuiver, M., Van Lent, J., Wellink, J., Van Kammen, A., 2000. Cowpea mosaic virus infection induces a massive proliferation of endoplasmic reticulum but not Golgi membranes and is dependent on de novo membrane synthesis. J. Virol. 74, 6556–6563.

Carrington, J.C., Freed, D.D., Oh, C.-S., 1990. Expression of potyviral polyproteins in transgenic plants reveals three proteolytic activities required for complete processing. EMBO J. 9, 1347–1353.

Chiu, W.L., Niwa, Y., Zeng, W., Hirano, T., Kobayashi, H., Sheen, J., 1996. Engineered GFP as a vital reporter in plants. Curr. Biol. 6, 325–330.

Collings, D.A., Carter, C.N., Rink, J.C., Scott, A.C., Wyatt, S., Allen, N.S., 2000. Plant nuclei can contain extensive grooves and invaginations. Plant Cell 12, 2425–2439.

den Boon, J.A., Chen, J., Ahlquist, P., 2001. Identification of sequences in brome mosaic virus replicase protein 1a that mediate association with endoplasmic reticulum membranes. J. Virol. 75, 12370–12381.

dos Reis Figueira, A., Golem, S., Goregaoker, S.P., Culver, J.N., 2002. A nuclear localization signal and a membrane association domain contribute to the cellular localization of the Tobacco mosaic virus 126-kDa replicase protein. Virology 301, 81–89.

Dunoyer, P., Ritzenthaler, C., Hemmer, O., Michler, P., Fritsch, C., 2002. Intracellular localization of the *Peanut clump virus* replication complex in tobacco BY-2 protoplasts containing green fluorescent protein-labeled endoplasmic reticulum or Golgi apparatus. J. Virol. 76, 865–874.

Fliegel, L., Burns, K., MacLennan, D.H., Reithmeier, R.A.F., Michalak, M., 1989. Molecular cloning of the high affinity calcium-binding protein (calreticulin) of skeletal muscle sarcoplasmic reticulum. J. Biol. Chem. 264, 21522–21528.

Fontes, E.B.P., Shank, B.B., Wrobel, R.L., Moose, S.P., O'Brian, G.R., Wurtzel, E.T., Boston, R.S., 1991. Characterization of an immunoglobulin binding protein homolog in the maize floury-2 endosperm mutant. Plant Cell 3, 483–496.

Fricker, M., Hollinshead, M., White, N., Vaux, D., 1997. Interphase nuclei of many mammalian cell types contain deep, dynamic, tubular membrane-bound invaginations of the nuclear envelope. J. Cell Biol. 136, 531–544.

Hagiwara, Y., Komoda, K., Yamanaka, T., Tamai, A., Meshi, T., Funada, R., Tsuchiya, T., Naito, S., Ishikawa, M., 2003. Subcellular localization

of host and viral proteins associated with tobamovirus RNA replication. EMBO J. 22, 344–353.
Haseloff, J., Siemering, K.R., Prasher, D.C., Hodge, S., 1997. Removal of a cryptic intron and subcellular localization of green fluorescent protein are required to mark transgenic *Arabidopsis* plants brightly. Proc. Natl. Acad. Sci. U.S.A. 94, 2122–2127.
Horsley, D., Coleman, J., Evans, D., Crooks, K., Peart, J., Satiat-Jeunemaitre, B., Hawes, C., 1993. A monoclonal antibody, JIM 84, recognizes the Golgi apparatus and plasma membrane in plant cells. J. Exp. Bot. 44, 223–229.
Janda, M., Ahlquist, P., 1993. RNA-dependent replication, transcription, and persistence of brome mosaic virus RNA replicons in *S. cerevisiae*. Cell 72, 961–970.
Kim, K.-H., 1993. Ph.D. Ribosomal Frameshift Regulation of Viral Polymerase: Red Clover Necrotic Mosaic Virus as a Model System. NC State University, Raleigh, NC.
Kim, K.H., Lommel, S.A., 1994. Identification and analysis of the site of −1 ribosomal frameshifting in red clover necrotic mosaic virus. Virology 200, 574–582.
Knebel, W., Quader, H., Schnepf, E., 1990. Mobile and immobile endoplasmic reticulum in onion bulb epidermis cells: short- and long-term observations with a confocal laser scanning microscope. Eur. J. Cell Biol. 52, 328–340.
Kong, L.J., Hanley-Bowdoin, L., 2002. A geminivirus replication protein interacts with a protein kinase and a motor protein that display different expression patterns during plant development. Plant Cell 14, 1817–1832.
Lee, W.-M., Ishikawa, M., Ahlquist, P., 2001. Mutation of host Δ-9 fatty acid desaturase inhibits brome mosaic virus RNA replication between template recognition and RNA synthesis. J. Virol. 75, 2097–2106.
Lui, P.P.Y., Kong, S.K., Kwok, T.T., Lee, C.Y., 1998. The nucleus of HeLa cell contains tubular structures for Ca^{2+} signalling. Biochem. Biophys. Res. Commun. 247, 88–93.
Mas, P., Beachy, R.N., 1999. Replication of tobacco mosaic virus on endoplasmic reticulum and role of the cytoskeleton in intercellular distribution of viral RNA. J. Cell Biol. 147, 945–958.
Miller, D.J., Schwartz, M.D., Ahlquist, P., 2001. Flock house virus RNA replicates on outer mitochondrial membranes in Drosophila cells. J. Virol. 75, 11664–11676.
Miller, D.J., Schwartz, M.D., Dye, B.T., Ahlquist, P., 2003. Engineered retargeting of viral RNA replication complexes to an alternative intracellular membrane. J. Virol. 77, 12193–12202.
Nebenführ, A., Gallagher, L.A., Dunahay, T.G., Frohlick, J.A., Mazurkiewicz, A.M., Meehl, J.B., Staehelin, L.A., 1999. Stop-and-go movements of plant Golgi stacks are mediated by the acto-myosin system. Plant Physiol. 121, 1127–1141.
Negrutiu, I., Shillito, R., Potrykus, I., Biasini, G., Sala, F., 1987. Hybrid genes in the analysis of transformation conditions. I. Setting up a simple method for direct gene transfer in plant protoplasts. Plant Mol. Biol. 8, 363–373.
Oparka, K., Boevink, P., Santa Cruz, S., 1996. Studying the movement of plant viruses using green fluorescent protein. Trends Plant Sci. 1, 412–418.
Osman, T.A.M., Buck, K.W., 1987. Replication of red clover necrotic mosaic virus RNA in cowpea protoplasts: RNA-1 replicates independently of RNA-2. J. Gen. Virol. 68, 289–296.
Paje-Manalo, L.L., Lommel, S.A., 1989. Independent replication of red clover necrotic mosaic virus RNA-1 in electroporated host and nonhost *Nicotiana* species protoplasts. Phytopathology 79, 457–461.
Petty, I.T.D., Hunter, B.G., Wei, N., Jackson, A.O., 1989. Infectious barley stripe mosaic virus RNA transcribed in vitro from full length genomic cDNA clones. Virology 171, 342–349.
Pokrovskaya, I.D., Gurevich, V.V., 1994. In vitro transcription: preparative RNA yields in analytical scale reactions. Anal. Biochem. 220, 420–423.
Reichel, C., Beachy, R.N., 1998. Tobacco mosaic virus infection induces severe morphological changes of the endoplasmic reticulum. Proc. Natl. Acad. Sci. U.S.A. 95, 11169–11174.
Restrepo-Hartwig, M., Ahlquist, P., 1999. Brome mosaic virus RNA replication proteins 1a and 2a colocalize and 1a independently localizes on the yeast endoplasmic reticulum. J. Virol. 73, 10303–10309.
Ritzenthaler, C., Nebenführ, A., Movafeghi, A., Stussi-Garaud, C., Behnia, L., Pimpl, P., Staehelin, L.A., Robinson, D.G., 2002. Reevaluation of the effects of brefeldin A on plant cells using tobacco Bright Yellow 2 cells expressing Golgi-targeted green fluorescent protein and COPI antisera. Plant Cell 14, 237–261.
Rohozinski, J., Hancock, J.M., 1996. Do light induced pH changes within the chloroplast drive turnip yellow mosaic virus assembly? J. Gen. Virol. 77, 163–165.
Rubino, L., Russo, M., 1998. Membrane targeting sequences in tombusvirus infections. Virology 252, 431–437.
Rubino, L., Di Franco, A., Russo, M., 2000. Expression of a plant virus non-structural protein in *Saccharomyces cerevisiae* causes membrane proliferation and altered mitochondrial morphology. J. Gen. Virol. 81, 279–286.
Rubino, L., Weber-Lotfi, F., Dietrich, A., Stussi-Garaud, C., Russo, M., 2001. The open reading frame 1-encoded ('36K') protein of Carnation Italian ringspot virus localizes to mitochondria. J. Gen. Virol. 82, 29–34.
Sanford, J.C., Smith, F.D., Russell, J.A., 1993. Optimizing the biolistic process for different biological applications. Methods Enzymol. 217, 483–509.
Schaad, M.C., Jensen, P.E., Carrington, J.C., 1997. Formation of plant RNA virus replication complexes on membranes: role of an endoplasmic reticulum-targeted viral protein. EMBO J. 16, 4049–4059.
Schlegel, A., Giddings, T.H., Ladinsky, M.S., Kirkegaard, K., 1996. Cellular origin and ultrastructure of membranes induced during poliovirus infection. J. Virol. 70, 6576–6588.
Scholthof, K.-B.G., Scholthof, H.B., Jackson, A.O., 1995. The tomato bushy stunt virus replicase proteins are coordinately expressed and membrane associated. Virology 208, 365–369.
Scholthof, H.B., Scholthof, K.-B.G., Jackson, A.O., 1996. Plant virus gene vectors for transient expression of foreign proteins in plants. Annu. Rev. Phytopathol. 34, 299–323.
Schwartz, M., Chen, J., Janda, M., Sullivan, M., den Boon, J., Ahlquist, P., 2002. A positive-strand RNA virus replication complex parallels form and function of retrovirus capsids. Mol. Cell 9, 505–514.
Selling, B.H., Allison, R.F., Kaesberg, P., 1990. Genomic RNA of an insect virus directs synthesis of infectious virions in plants. Proc. Natl. Acad. Sci. U.S.A. 87, 434–438.
Sit, T.L., Vaewhongs, A.A., Lommel, S.A., 1998. RNA-mediated transactivation of transcription from a viral RNA. Science 281, 829–832.
Staehelin, L.A., 1997. The plant ER: a dynamic organelle composed of a large number of discrete functional domains. Plant J. 11, 1151–1165.
Terasaki, M., Reese, T.S., 1992. Characterization of endoplasmic reticulum by co-localization of BiP and dicarbocyanine dyes. J. Cell. Sci. 101, 315–322.
Vaewhongs, A.A., Lommel, S.A., 1995. Virion formation is required for the long-distance movement of red clover necrotic mosaic virus in movement protein transgenic plants. Virology 212, 607–613.
van Regenmortel, M., Fauquet, C.M., Mayo, M.A., Bishop, D.H.L. (Eds.), 1999. Virus Taxonomy. Seventh Report of the International Committee on Taxonomy of Viruses. Academic Press, New York, pp. 805–808.
Weber-Lotfi, F., Dietrich, A., Russo, M., Rubino, L., 2002. Mitochondrial targeting and membrane anchoring of a viral replicase in plant and yeast cells. J. Virol. 76, 10485–10496.
Wee, E.G.-T., Sherrier, D.J., Prime, T.A., Dupree, P., 1998. Targeting of active sialyltransferase to the plant Golgi apparatus. Plant Cell 10, 1759–1768.
Wijkamp, I., van Lent, J., Kormelink, R., Goldbach, R., Peters, D., 1993. Multiplication of tomato spotted wilt virus in its insect vector, *Frankliniella occidentalis*. J. Gen. Virol. 74, 341–349.
Wrobel, R.L., OBrian, G.R., Boston, R.S., 1997. Comparative analysis of BiP gene expression in maize endosperm. Gene 204, 105–113.
Xiong, Z., Lommel, S.A., 1989. The complete nucleotide sequence and

genome organization of red clover necrotic mosaic virus RNA-1. Virology 171, 543–554.

Xiong, Z., Kim, K.H., Giesman-Cookmeyer, D., Lommel, S.A., 1993a. The roles of the red clover necrotic mosaic virus capsid and cell-to-cell movement proteins in systemic infection. Virology 192, 27–32.

Xiong, Z., Kim, K.H., Kendall, T.L., Lommel, S.A., 1993b. Synthesis of the putative red clover necrotic mosaic virus RNA polymerase by ribosomal frameshifting in vitro. Virology 193, 213–221.

Zavriev, S.K., Hickey, C.M., Lommel, S.A., 1996. Mapping of the red clover necrotic mosaic virus subgenomic RNA. Virology 216, 407–410.